

# Hydrodynamic response of a submerged tunnel element suspended from a twin-barge under random waves

Can Yang <sup>a,b</sup>, Sam D. Weller <sup>b</sup>, Yong-xue Wang <sup>a</sup>, De-zhi Ning <sup>a</sup>, Lars Johanning <sup>b,a,\*</sup>

<sup>a</sup> State Key Laboratory of Coastal and Offshore Engineering, Dalian University of Technology (DUT), Dalian 116024, China

<sup>b</sup> College of Engineering, Mathematics and Physical Sciences, University of Exeter, Penryn Campus, Penryn, Cornwall, TR10 9FE, UK

---

**Abstract:** It is possible that the excessive dynamic responses of tunnel elements could jeopardize the safety and accuracy of installation procedures used during subsea tunnel construction. To investigate the motion characteristics of the tunnel element, experimental measurements of a moored tunnel element suspended from a twin-barge were conducted in a wave flume at a geometric scale of 1:50. A corresponding numerical model was developed to simulate the dynamic response of the tunnel-barge system in realistic sea conditions, using hydrodynamic parameters from a radiation/diffraction potential model. Multiple linear wave conditions and three immersion depths were tested. The results indicate that the motion response of the tunnel element increases with decreasing immersion depth, and the natural periods of the tunnel, barge and combined tunnel-barge system play key roles in the influence of wave conditions on the motions of the tunnel. It was found that the low-frequency motion of the tunnel element is large in small wave periods. The mooring system under such conditions needs to be considered carefully during system design in order to safely control the motions of the tunnel-barge system in energetic ocean environments.

**Key words:** Immersed tunnel; Twin-barge; Motion response; Irregular waves; Numerical model

## 1. Introduction

It is widely acknowledged that the underwater transportation of tunnel elements has a significant role to play in reducing cross-sea traffic and transit times in busy shipping areas. There are several advantages to using this form of tunnel structure including; the ability to construct tunnel elements onshore, the reduced time required onsite, definite stress characteristics and lower buried depth compared with the shield method (Fu 2004; Guan 2004). For these reasons the immersed tunnel element approach has been successfully and widely used in large scale underwater tunnel projects (e.g. (Li et al. 2003)). Transportation and lowering of the tunnel elements are critical installation procedures requiring a detailed understanding of the behavior of each structural element (Kasper et al. 2008). In offshore locations subjected to changeable weather and extreme waves, the environmental conditions will affect the behavior of tunnel element and its mooring during installation, necessitating accurate control of vessel position.

\* Corresponding author (Lars Johanning). Tel.: 0044 (0)1326 253730; fax: 0044 (0)1326 371859. E-mail address: L.Johanning@exeter.ac.uk.

In addition, during towing from the onshore dockyards to the installation site the constructed elements are typically suspended by barges, pontoons or elevating platforms (Chen et al. 2009). Once on station above the trench, onboard winches and suspension lines are used to control the sinking process. During installation the onset of severe environmental conditions, due to wind, wave and current, could result in interruption of the operation with the immersed tunnel element in a stationary position (Janssen et al. 2006). In this situation safe station keeping is the main concern, and the motion response of the barge and tunnel element under these extreme environmental conditions needs to be understood. Hereby the behavior of the mooring system (used to keep the barge on station), and suspension system (that holds the tunnel element suspended from the barge) needs to be fully characterized, as both will directly influence the motion response of the coupled system. It is therefore prudent that a detailed hydrodynamic analysis of the moored tunnel and barge system is carried out considering a number of scenarios which represent a range of energetic ocean conditions.

Many research studies of immersed tunnel elements have been carried out in the past, and the majority of existing studies focus on the seismic response, underwater interfacing, structure anti-seismic and foundation treatment (Anastasopoulos et al. 2007; Grantz et al. 2001; Do et al. 2015; Li et al. 2014). Considerably less study has been directed at installation procedures and the hydrodynamic characteristics of the immersed tunnel element and its deployment barge still need to be investigated further. Zhou et al. (2001), Xiao et al. (2010) and Zhan et al. (2001) conducted experimental studies on the motion characteristics of immersed tunnel elements subjected to drag loading in rivers. Aono et al. (2003) investigated the stability of Japanese NaHa immersed tunnel elements in the foundation trench, focusing on the influence of different ballast water weights and wave factors and addressing sliding of the tunnel. Based on the Busan-Geoje Fixed Link in Korea, Partha et al. (2008) performed numerical analysis on the immersion process of the tunnel element using MOTSIM software and also simulated the dynamic response of the tunnel as it approached the seabed trench. Their results demonstrated that the negative buoyancy of the tunnel element (in the range of 1%-2.5%) directly effects the tension of the four suspension cables. They concluded that in order to avoid slack suspension cables the negative buoyancy of tunnel element should reach 2.5%. Chen et al. (2012) and Peng et al. (2012) carried out numerical and experimental investigations on the dynamic response of tunnel-pontoon systems during an interruption in the lowering process, with the study based on the Hong Kong-Zhu Hai-Macao Bridge project. However, these investigations focused on hydrodynamic response of the tunnel element subjected to regular waves. Realistic seas comprise random waves and consequently studies of tunnel responses need consider the response of such systems in irregular waves.

The investigations presented here outline a series of physical model tests and numerical analysis which focused on the dynamic response of moored tunnel element suspended by a twin-barge subjected to irregular waves. The results presented in this paper build upon an earlier study by the authors (Yang et al., 2016). The experimental setup and typical test conditions are introduced in Section 2. The numerical validation procedure, decaying motion tests and simulation of the tunnel-barge system under irregular waves, are presented in Section 3. A comparison of experimental measurements with the outcomes from the numerical studies for three sea states are presented in Section 4. Finally conclusions and discussion on future work are provided in Section 5.

## 2. Summaries

### 2.1 Experimental setup

The model tests were conducted in the ocean environmental flume of the State Key Laboratory of Coastal and Offshore Engineering at Dalian University of Technology in China. A summary of the experimental setup is provided in this section but for further information the reader is directed to (Yang et al., 2016). The wave flume was 50m long, 3.0m wide and 1.0m deep (Fig.1a). A piston-type wave maker was used to generate the desired incident waves at one end of the flume with an absorbing device for wave dissipation at the other end of the flume. In Fig.1b a front view of the immersed tunnel element supported by the twin barge and suspension cables arranged is shown in the middle of the flume, in addition to the mooring lines which were used to anchor the tunnel element and barge system to the flume bottom.

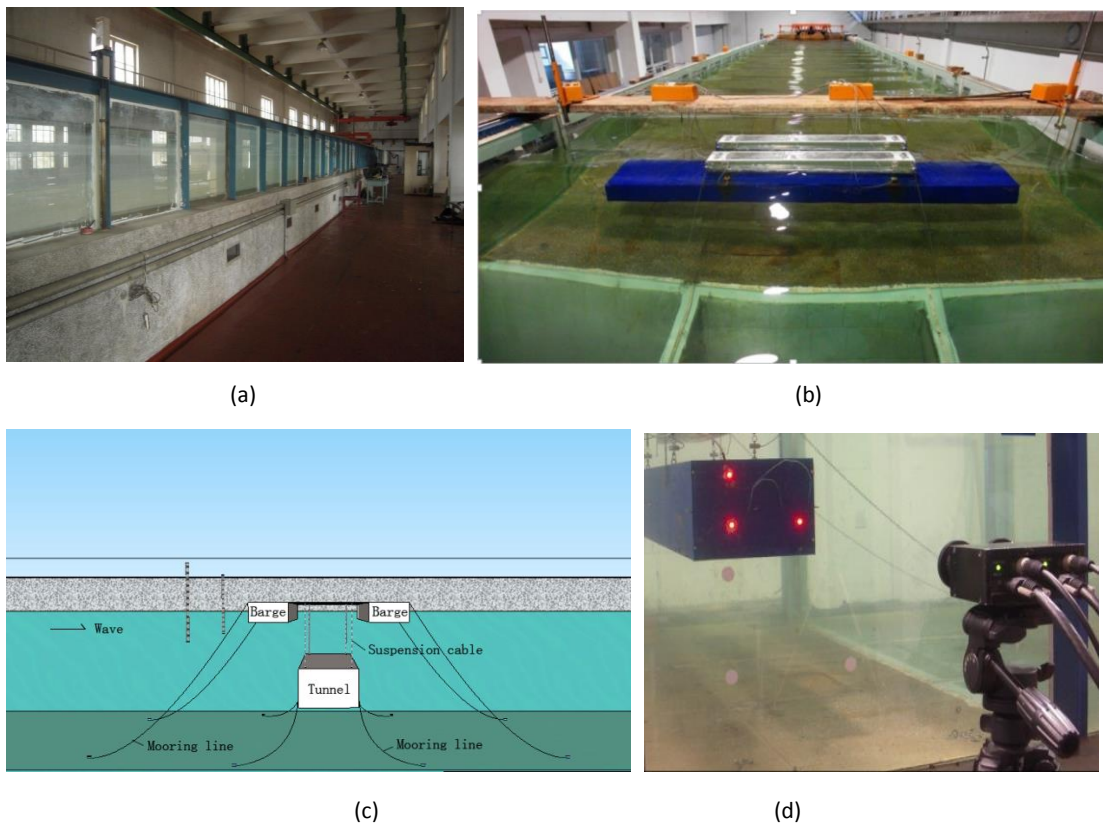


**Fig. 1.** (a) Wave-current flume used for the ocean environment test. (b) Front view of the tunnel element and barge models. (c) Sketch of the tunnel and barge mooring system. (d) Untouched 6-D Measurement System.

The tunnel element model was manufactured from cement mortar and reinforced with water resistant polymer on the tunnel's outer surface. The thickness of the concrete tunnel walls was set to obtain the correct model weight. The wave-induced motion of the twin-barges was also studied in these tests, with the barge models fabricated from two hollow and airtight cuboid floating barges joined by a connecting steel frame. The model scale of the tunnel element was determined by the tank dimensions, particularly its length and consequently a Froude scale factor of 1:50 was selected. The main parameters of immersed tunnel element and twin-barge model are listed in Table 1.

**Table 1**

Parameters of tunnel element and twin-barge model.

Component	Parameter	Value
Tunnel element	Length × Width × Height(m)	2×0.3×0.2
	Weight in air (N)	1200.5
	Weight in water (N)	1176
Twin-barge	Length × Width × Height(m)	1×0.2×0.095
	Weight in air (N)	172.5
	Draught (cm)	5.5

The 6 degree-of-freedom movements of the immersed tunnel element are heavily influenced by the motions of the twin-barge with loads transferred to the tunnel element via the suspension cables. Fig. 1c shows the arrangement of suspension cables and mooring lines of the tunnel-barge system used in the model tests. In this set of experiments thin wire ropes were selected to represent the suspension cables. Anchor chains with a representative scaled mass per unit length were used to simulate the mooring lines for the twin-barge. The axial elasticity of both suspension cables and mooring lines were represented by using calibrated linear springs with appropriate stiffness properties. Parameters of the mooring lines and suspension cables are provided in Table 2. It should further be noted that due to different submersion stages, the suspension cable length of the tunnel element was altered with the different immersion depths. Three spring force-extension curves for the different immersion depths are shown in Fig.2.

**Table 2**

Parameters of the mooring lines of tunnel element and twin-barge

Component	Parameter	Value
Suspension cable ( $d=0.3m$ )	Length (m)	0.34
	Elasticity coefficient (N/m)	$1.37 \times 10^3$
Mooring line of tunnel element	Length (m)	0.62
	Weight (kg/m)	$8.5 \times 10^{-2}$
	Stiffness (N/m)	$3.4 \times 10^3$
Mooring line of twin-barge	Length (m)	1.5
	Weight (kg/m)	$6.5 \times 10^{-2}$
	Stiffness (N/m)	$1.34 \times 10^3$

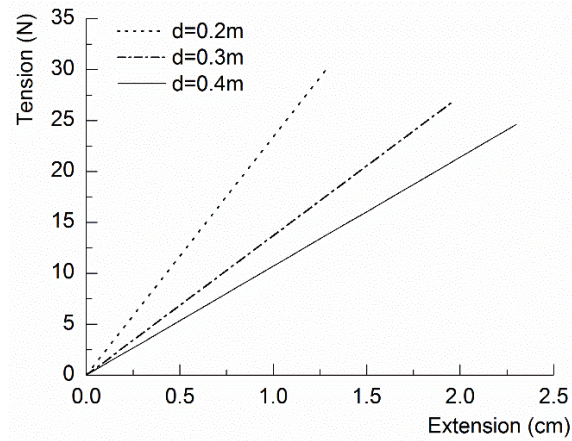


**Fig. 2.** Relationship between the elastic line force and spring extension

The motion response of the tunnel-barge system was monitored by the ‘Untouched 6-D Measurement System (6D-UMS)’ which based on the principle of binocular vision (Fig. 1d) (Yang et al., 2016). The sampling rate of the real-time measurement system was 30 Hz, the translation motion precision (surge, heave and sway) of the 6D-UMS can be controlled to be less than 0.3% full-scale (FS), and the precision of the rotation quantity (yaw, pitch and roll) can be controlled to be less than 1.2% FS.

## 2.2 Tests for comparison

According to the Froude similarity criterion used (1:50), the water depth in the flume was set to 0.8m, corresponding to a water depth of 40m at the hypothetical installation site. In order to avoid the combined effects of wave diffraction and reflection near the flume side in close proximity to the tunnel model, the minimum immersion depth and maximum significant wave height in the experiment were chosen as  $d=20\text{cm}$  and  $H_s=5\text{cm}$ , respectively. In this case the ratio of significant wave height and immersion depth is 0.25. In the tests the irregular waves were simulated (Fig. 3) and the wave conditions used for the comparison are listed in Table 3.

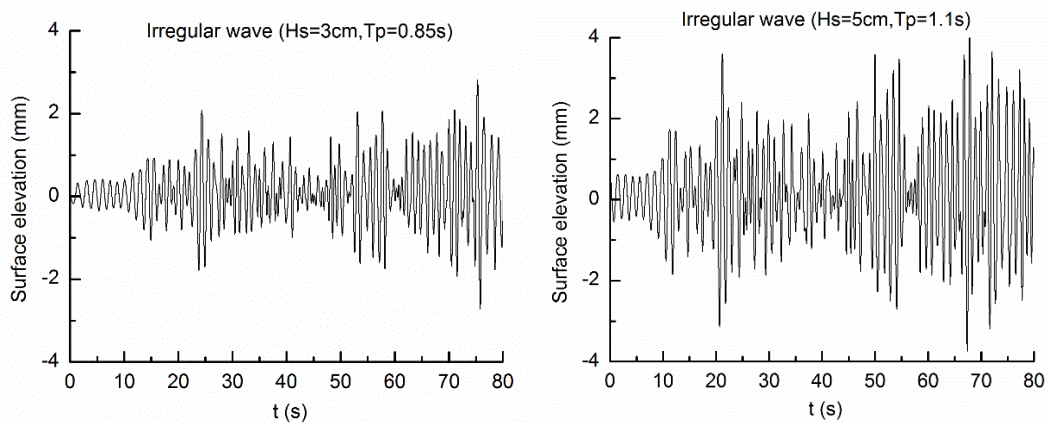


**Fig. 3.** Time series of measured surface elevation of irregular waves

**Table 3**

Environmental parameters under irregular wave conditions

Parameter	Model	Full scale
Immersion depth ( $d$ )	20cm	10m
	30cm	15m
	40cm	20m
Significant wave height ( $H_s$ )	3cm	1.5m
	4cm	2m
	5cm	2.5m
Peak period ( $T_p$ )	0.85s	6s
	1.0s	7s
	1.1s	8s
Incident wave direction ( $\theta$ )	90°	90°
Mooring line angle ( $\beta$ )	45°	45°

A single incident wave direction was used ( $\theta=0^\circ$ ). The significant wave height at full scale varied from 1.5 to 2.5m with a 0.5m interval and three wave peak periods as  $T_p=0.85s$ , 1.0s and 1.1s were considered (flume scale). In this experiment, the angle of mooring lines with the  $xyz$ -axis was fixed at  $\beta=45^\circ$  which, from a previous study (Yang et al 2014) was determined as the optimum arrangement of mooring lines for the system. A JONSWAP spectrum was chosen to simulate the targeted irregular waves with a peak enhancement factor of  $\gamma=3.3$ . The comparison curves of measured and target spectrum with three typical wave conditions agree well, as is shown in Fig. 4.

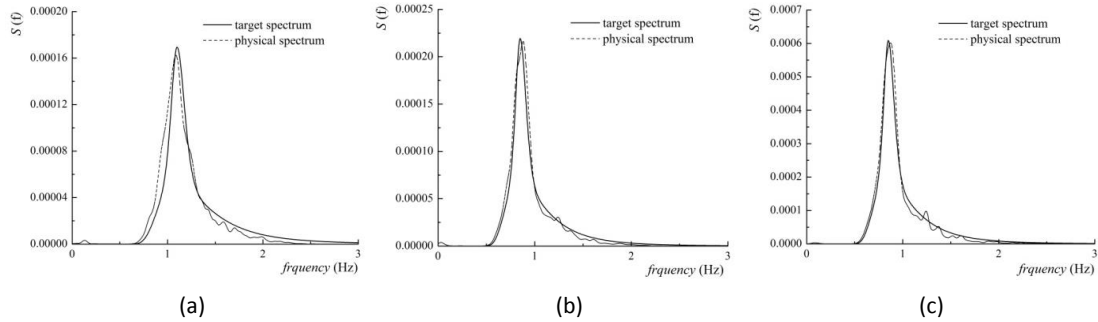


**Fig. 4** Comparison of measured and target spectrum with tested wave conditions: (a)  $H_s=3cm$ ,  $T_p=0.85s$ , (b)  $H_s=3cm$ ,  $T_p=1.1s$  and (c)  $H_s=5cm$ ,  $T_p=1.1s$ .

### 3. Modelling approach

A scaled numerical model of the tunnel element submerged by twin-barge was generated (see Fig. 5a and Fig. 5b). The coordinate system  $oxy$  is at the undisturbed water surface. The  $x$ -axis and  $y$ -axis are directed along the length (surge) and the width (sway) of the tunnel element, respectively, with the  $z$  coordinate orientated upwards as the positive direction. The incident waves propagate along the flume in the position  $y$  direction. The center of gravity (COG) of the experimental twin-barge model in free-floating conditions was at 0.025m below the static water level in the flume. The same draft of twin-barge was set in the numerical model. The coordinate of the mooring line attachment points (Fig.5c) of the tunnel-barge system in static water are detailed in Table 4.

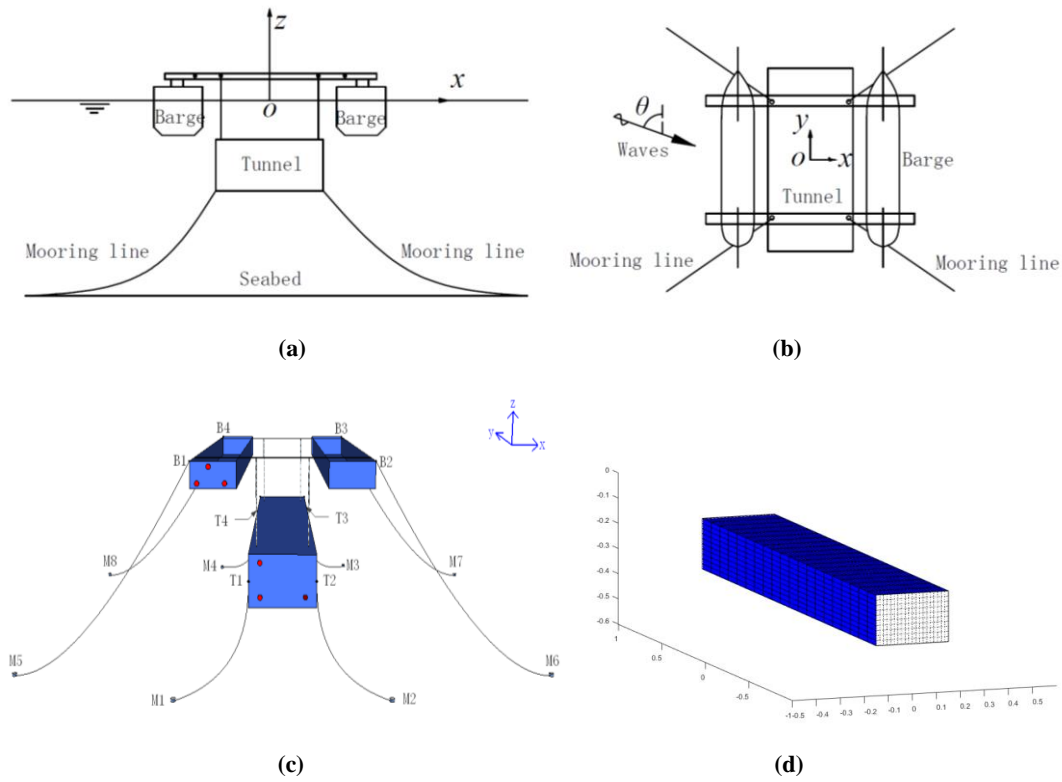


**Fig. 5.** Schematic diagram of numerical model of the immersed tunnel element

**Table 4**

Coordinate of the attachment and anchor points of mooring lines

Attachment point	Global coordinate (m)	Local coordinate (m)	Anchor point	Global coordinate (m)	Local coordinate (m)
T1	(-0.15, -1, -0.1-d)	(-0.15, -1, 0)	M1	(-0.43, -1.28, -0.8)	(-0.43, -1.28, d-0.7)
T2	(0.15, -1, -0.1-d)	(0.15, -1, 0)	M2	(0.43, -1.28, -0.8)	(0.43, -1.28, d-0.7)
T3	(0.15, 1, -0.1-d)	(0.15, 1, 0)	M3	(0.43, 1.28, -0.8)	(0.43, 1.28, d-0.7)
T4	(-0.15, 1, -0.1-d)	(-0.15, 1, 0)	M4	(-0.43, 1.28, -0.8)	(-0.43, 1.28, d-0.7)
B1	(-0.1, -0.5, 0.04)	(-0.1, -0.5, 0.05)	M5	(-1.55, -1, -0.8)	(-1.25, -1, -0.79)
B2	(0.7, -0.5, 0.04)	(0.7, -0.5, 0.05)	M6	(1.55, -1, -0.8)	(1.85, -1, -0.79)
B3	(0.7, 0.5, 0.04)	(0.7, 0.5, 0.05)	M7	(1.55, 1, -0.8)	(1.85, 1, -0.79)
B4	(-0.1, 0.5, 0.04)	(-0.1, 0.5, 0.05)	M8	(-1.55, 1, -0.8)	(-1.25, 1, -0.79)

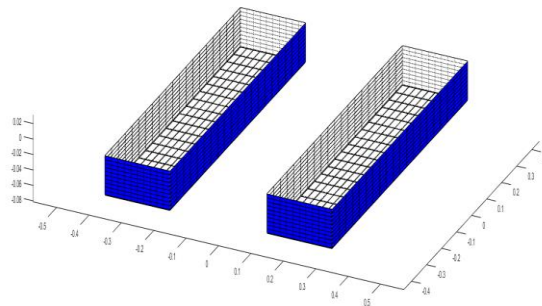


**Fig. 6.** Twin-barge mesh used for the diffraction/radiation potential analysis

The hydrodynamic properties of simplified twin-barge and tunnel element model were calculated by the diffraction/radiation potential code WAMIT, and used by the time-domain mooring modelling tool Orcaflex™ to simulate the dynamic response of the coupled system. Matlab was used to calculate the mesh of both tunnel and twin-barge, utilizing the symmetry of these geometries about the x- and y-axis (Fig. 5d). For hydrodynamic parameter calculation the twin-barge mesh does not include the connecting steel frame which connected the two floating barges (Fig. 6), because it was observed during the experimental tests that this part of the system remained above the free water surface. The 6 degrees of freedom of the tunnel and twin-barge model were calculated in a similar approach as described by (Harnois et al 2014) using the frequency-dependent data, which are: a) the values of the radiation damping at the center of gravity (COG) of the tunnel (barge), b) the added masses at the COG of the tunnel and c) the load Response Amplitude Operators (RAOs) and associated phases at the metacenter at the equilibrium position of the tunnel (barge). The relative parameters and the main properties of tunnel-barge system in the numerical model are listed in Table 5.

**Table 5**

Properties of full scale and model tunnel element and difference with theoretical values.

Parameter	Full scale values	Theoretical scaled values	Measured scaled values	Relative error
Mass of tunnel (t)	15321.5	0.1225	0.1225	0%
Moment of inertia $I_{xx}$ (t m <sup>2</sup> )	$1.28 \times 10^7$	0.041	0.043	4.65%
Moment of inertia $I_{yy}$ (t m <sup>2</sup> )	$4.15 \times 10^5$	0.0013	0.0014	7.14%
Moment of inertia $I_{zz}$ (t m <sup>2</sup> )	$1.3 \times 10^7$	0.042	0.045	6.67%

### 3.1 Decaying motion tests

To study the natural frequencies of tunnel-barge system, a series of experimental decay tests of the tunnel, twin-barge and tunnel-barge system were carried out in static water. In order to do this an offset from the equilibrium position of each case were implemented for each degree of freedom with the decaying motion monitored by the 6D-UMS. For the coupled mode of the tunnel-barge system, take sway motion as an example, decay tests involved moving the moored twin-barge (and due to the connection provided by the suspension cables; the tunnel element) from its equilibrium position in the sway direction and then releasing the twin-barge. Prior to release wave disturbance was kept to a minimum. The tunnel element and the twin-barge move at their natural frequencies for this degree of freedom, and the motion amplitude decreases because of the system damping. It is acknowledged that motions in other degrees of freedom would have been present in the decaying response. The damping of the tunnel-barge system was evaluated by measuring the total damping in the decay motion tests without the mooring lines attached. For the tests of the single tunnel, springs were attached to the suspension cables between the tunnel and a fixed structural frame over the flume. Three different spring stiffness  $k_s=1.07 \times 10^3$ ,  $1.37 \times 10^3$  and  $2.34 \times 10^3$  N/m were used for each immersion depths listed in Table 3.

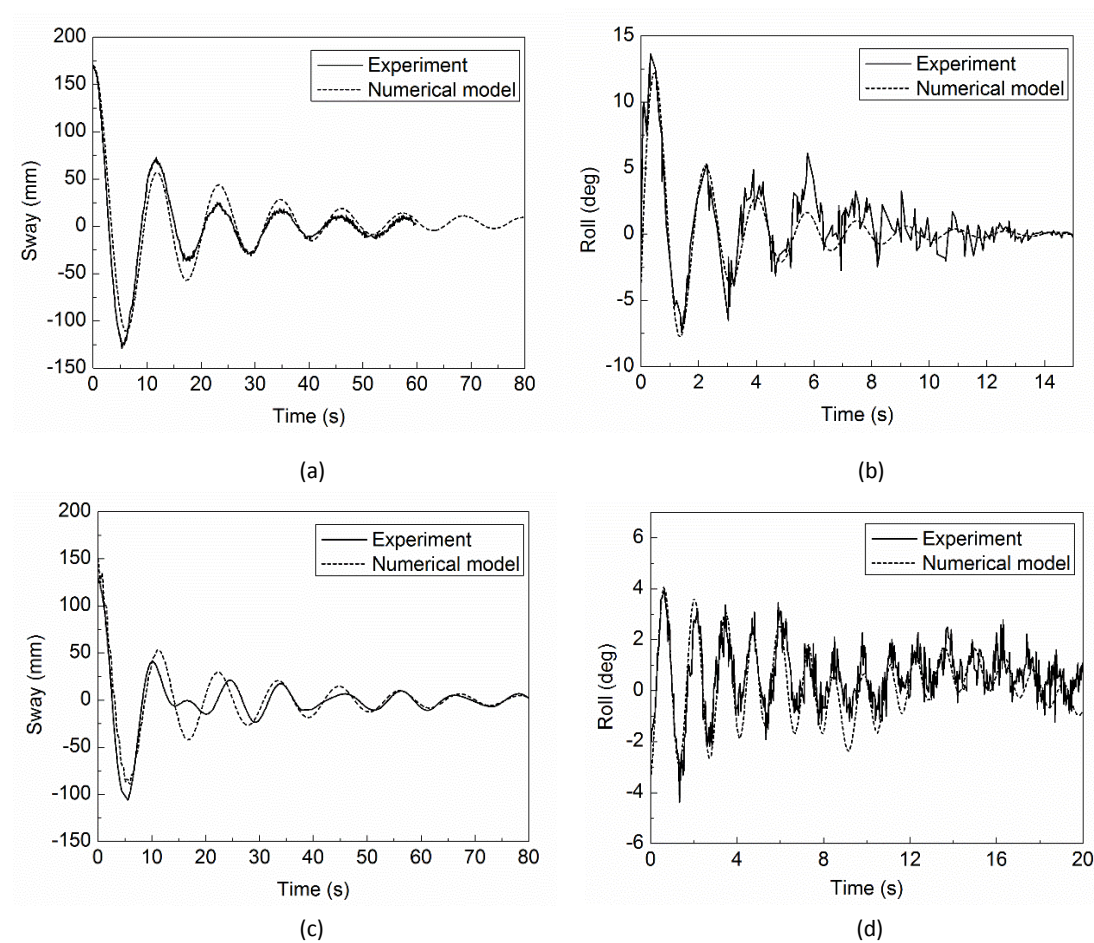
The natural frequency and damping of moored tunnel-barge system were evaluated from the decaying motion tests and also simulated using the numerical model. Fig. 7 shows the simulated decay tests of single twin-barge, single tunnel and tunnel-barge system calculated for the 0.4m immersion depth case. Comparatively the numerical and experimental results of the decaying motion in sway, heave and roll directions agree very well, with the numerical model able to



replicate the measured decay motion amplitude of the system, albeit with an apparent underestimation of linear and quadratic damping. Additional quadratic and linear damping terms were introduced to the numerical model iteratively to improve the simulated response, as is shown in Table 6. The quadratic damping  $p_1$  and linear damping  $p_2$  are the additional damping coefficients involved in the formulation below:

$$\begin{aligned}
 F_x &= -p_{1sway} V_x |V_x| - p_{2sway} V_x \\
 F_y &= -p_{1surge} V_y |V_y| - p_{2surge} V_y \\
 F_z &= -p_{1heave} V_z |V_z| - p_{2heave} V_z \\
 M_x &= -p_{1pitch} \Omega_x |\Omega_x| - p_{2pitch} \Omega_x \\
 M_y &= -p_{1roll} \Omega_y |\Omega_y| - p_{2roll} \Omega_y \\
 M_z &= -p_{1yaw} \Omega_z |\Omega_z| - p_{2yaw} \Omega_z
 \end{aligned} \tag{1}$$

where  $V$  is the translational velocity,  $\Omega$  is the angular velocity,  $F$  and  $M$  are the damping force and moment, respectively.



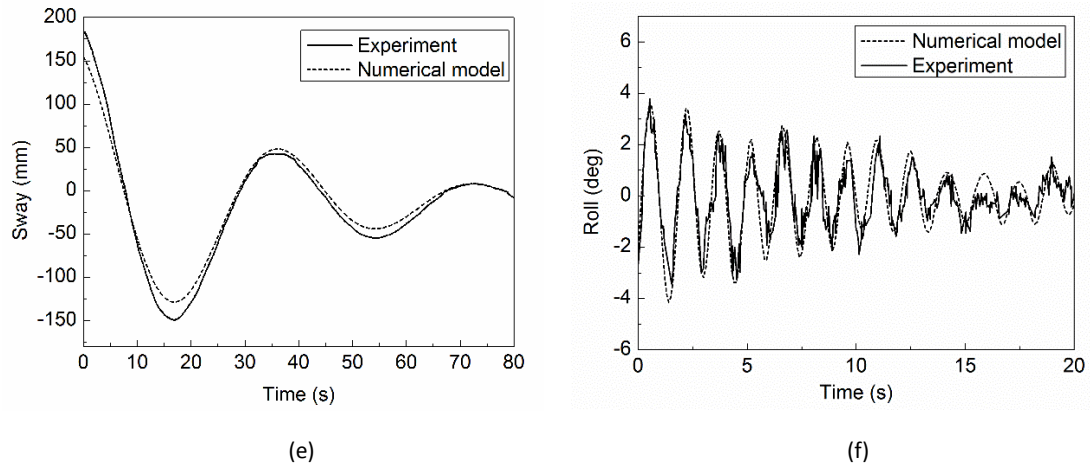


**Fig. 7.** Time histories of measured and numerical decay tests in a) sway, for single barge; b) sway, for single tunnel; c) sway, for tunnel-barge system; and d) roll, for single barge; e) roll, for single tunnel; f) roll, for tunnel-barge system.

**Table 6**

Additional quadratic and linear damping for the sway motion applied to the numerical model.

system	Additional quadratic damping $p_1$ (KN·s <sup>2</sup> ·m <sup>-2</sup> )	Additional linear damping $p_2$ (KN·s·m <sup>-1</sup> )
Tunnel	0.3968	0.0132
Twin-barge	0.0128	0.0021

In sway direction the immersion depth of the tunnel does not have much effect on the natural frequency of tunnel and tunnel-barge system. The natural frequencies of the barge and tunnel when tested individually are relatively close, but the natural period of the combined tunnel-barge system is clearly a lot larger (Fig. 7a, 7c and 7d). This difference illustrates that when combined, the tunnel and barge interact with each other and increase the period of motion. As shown in Table 7, due to the larger weight of tunnel, the heave natural frequency of tunnel-barge system is more close to the tunnel element and is larger than for the individual barge. When the single tunnel roll response is compared to that of the tunnel-barge system it is clear that the latter system's natural frequency is influenced by the significant overturning resistance of the supporting twin-barge.

**Table 7**

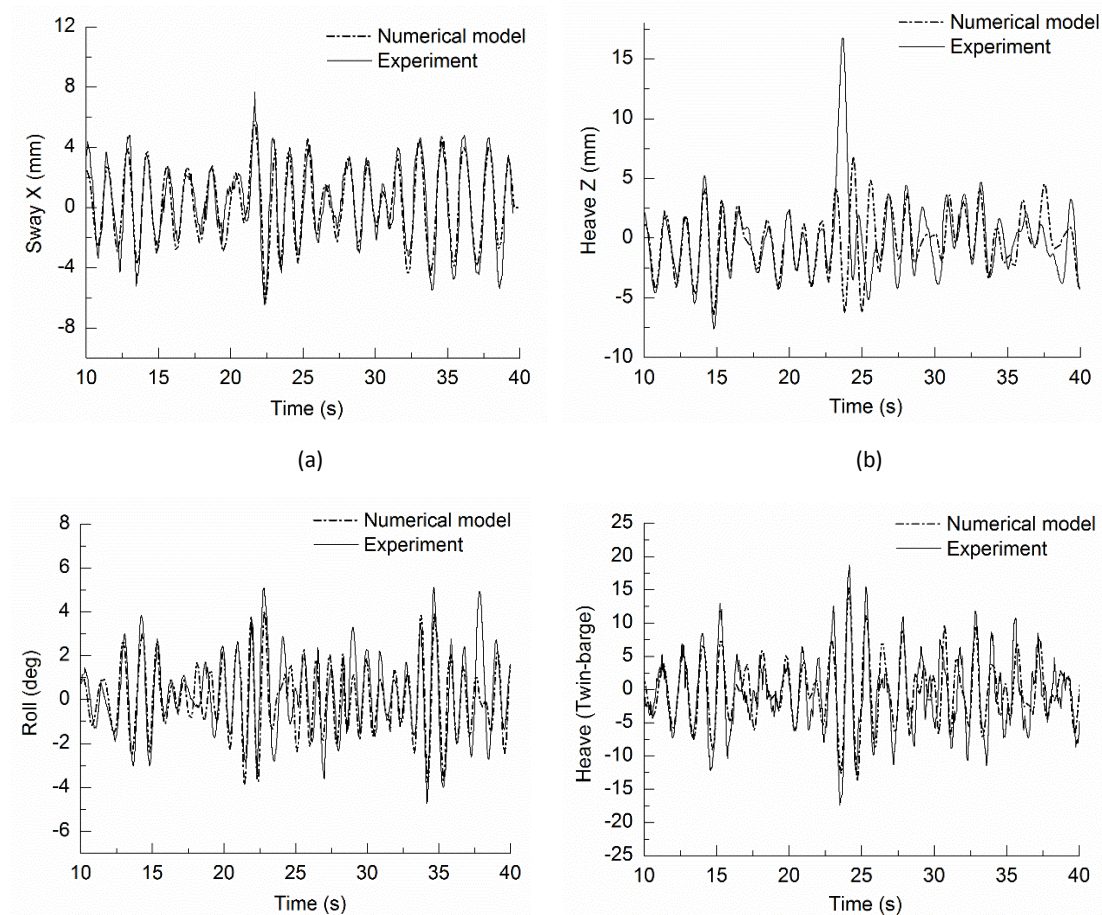
The free vibration period of the tunnel and twin-barge in static water

Values of natural period		Single barge	Single tunnel	Tunnel-barge system
Sway (Hz)	Numerical values	0.0872	0.0891	0.0265
	Measured values	0.0881	0.0897	0.0269
	Relative error	1.05%	0.71%	1.85%
Heave(Hz)	Numerical values	1.02	0.243	0.348
	Measured values	1.064	0.25	0.359
	Relative error	4.08%	2.67%	3.13%
Roll (Hz)	Numerical values	0.571	0.741	0.897
	Measured values	0.598	0.763	0.873
	Relative error	4.57%	6.42%	2.75%

### 3.2 Irregular wave tests

Irregular wave tests aim to evaluate the hydrodynamic motions of the tunnel element subjected to realistic sea conditions. The free surface elevation measured (at 50Hz) during the experimental test was used directly in the numerical model in order to validate the model in irregular wave conditions. This time series was not modified for the Orcaflex model in order to adequately represent the measured conditions.

Fig. 8 provides a comparison of the measured and simulated tunnel motion time histories with  $H_S=3\text{cm}$  and  $T_P=1.1\text{s}$ . With the measured irregular wave elevation input in the numerical model, very good agreement was achieved in the sway and roll directions. The only significantly lower correlation coefficient of the fit can be observed for the measured heave time series at around 24s. In order to investigate the cause of this sudden, large amplitude motion, detailed time series from 20s to 30s of the synchronous measured tunnel motions, twin-barge motions and suspension cable tensions are shown in Fig.9. In addition the measured and simulated floating twin-barge heave motions and suspension cable loads are shown in Fig. 8 d and Fig.10, respectively. It can be seen from Fig. 9 that the suddenly intense movement of the tunnel element at 23s occurred due to the relatively large motion responses of twin-barge in the previous two oscillation cycles. Corresponding large amplitude suspension cable loads were also measured during this interval, but these were not simulated, hence the lack of large amplitude heave peak for the tunnel.



(c)

(d)

**Fig. 8.** Validation of time series of the motion responses between experimental and modelling results

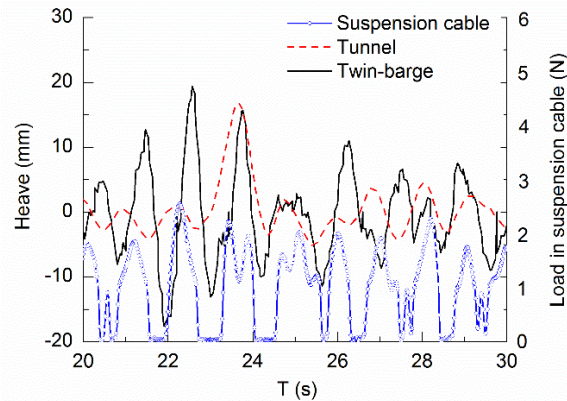


**Fig. 9.** Detailed time series of tunnel motions, twin-barge motions and suspension cable tensions

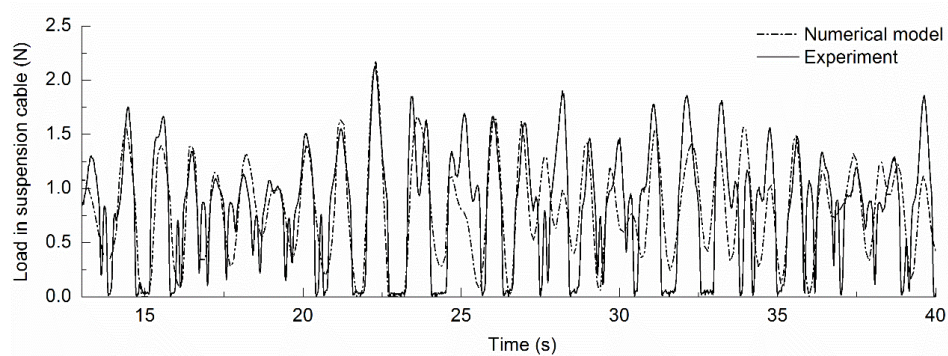


**Fig. 10.** Validation of suspension cable load time series of the tunnel element between experimental and numerical results

#### 4. Results and discussion

Figs. 11-13 show the motion response amplitudes of the tunnel element under different irregular wave conditions over an interval of approximately 100 waves. The maximum and minimum movement displacements were used to calculate the motion amplitudes of the tunnel were statistically extracted, focusing on the highest 1/3 motion amplitudes. In the numerical model, JONSWAP spectrum was used to simulate the targeted irregular waves with a peak enhancement factor of  $\gamma=3.3$  (Sarpkaya and Isaacson, 1981). The results are discussed in detail below.

##### 4.1 Effect of wave period on the tunnel motions

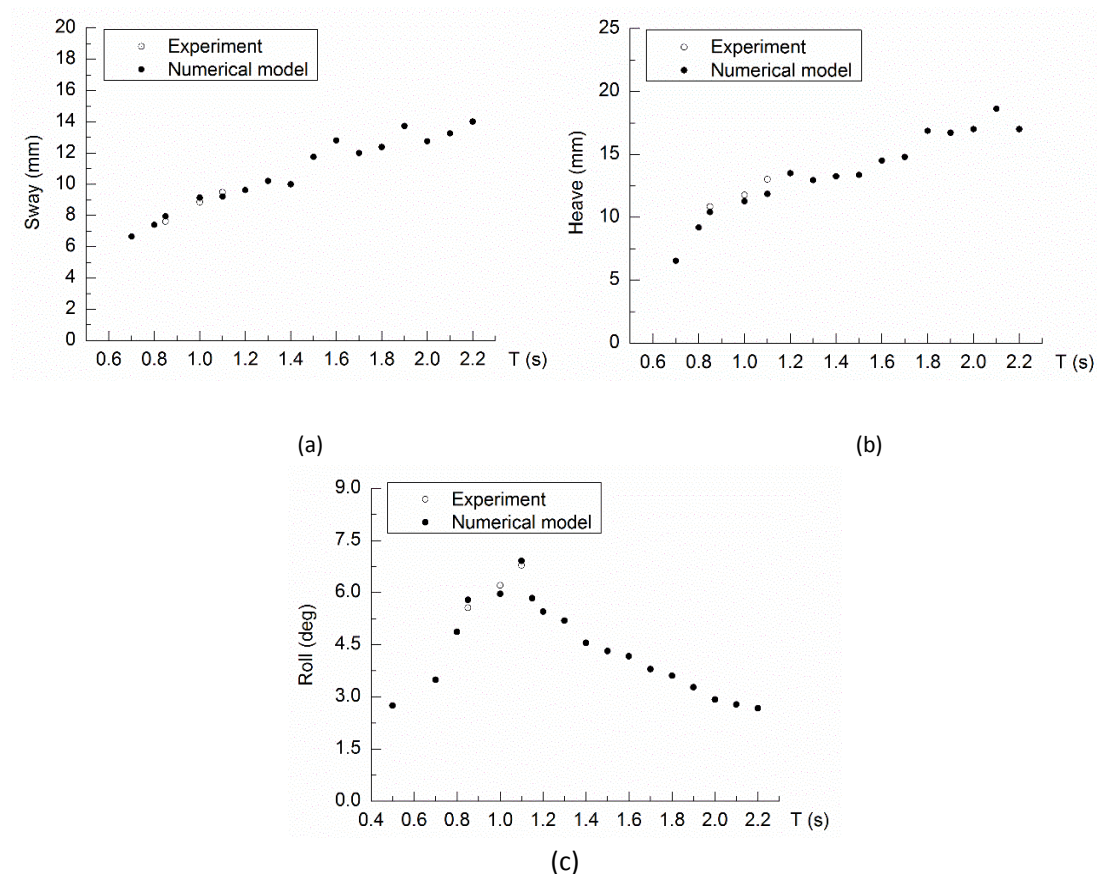
Various scenarios were considered to characterise the motion response of the tunnel element in terms of wave period, wave height and immersion depth. This study focused on high-frequency (wave frequency) motion of the tunnel element were chosen to investigate the effect of wave conditions on tunnel motions.

Fig. 11 shows the statistical amplitude of tunnel motions with different peak frequency periods with a significant wave height of 0.05m. To be conservative, wave periods between 0.7s to



2.2s were selected, to cover a range of extreme conditions. It can be seen from the figure that the motion amplitude of the tunnel element increases with increasing wave peak frequency period for both the sway and heave modes.

In the roll direction, the tunnel motion amplitudes increase with increasing wave period until a maximum is reached at  $T_p = 1.1s$ . For higher periods the tunnel roll amplitudes decrease with increasing wave period. Compared to an earlier study (Yang et al. 2015) in which a submerged tunnel element was subjected to wave loading without being suspended by a twin-barge, the response of the tunnel in this study is notably different. This demonstrates that the motion response of the entire coupled system must be considered rather than just the tunnel element alone. Meanwhile, Table 7 and Fig. 7f shows the roll natural frequency of the tunnel-barge system is around 0.9Hz, and Fig. 11c shows that the peak value of tunnel roll motions occurs around  $T_p = 1.1s$ . As expected, this indicates that the tunnel response amplitudes are largest when the moored tunnel-barge system natural period is close to the incident wave peak period.



**Fig. 11.** Motion amplitudes of immersed tunnel element suspended by twin-barge for different wave peak periods

#### 4.2 Effect of significant wave height on the tunnel motions

The statistical amplitude of the tunnel motions are plotted against significant wave height with the fixed immersion depth of 0.2m for several wave periods ranging from 0.7-1.3s. Three significant wave heights  $H_s = 3cm, 4cm$  and  $5cm$  were considered in the numerical model. It can be observed from Fig. 12 that the tunnel amplitudes increase approximately linearly with the significant wave height for the sway and heave modes, and also for small wave periods ( $T_p < 1.1s$ ) in

the roll direction. This general trend is also expected with wave loading on the tunnel-barge system increasing with wave height.

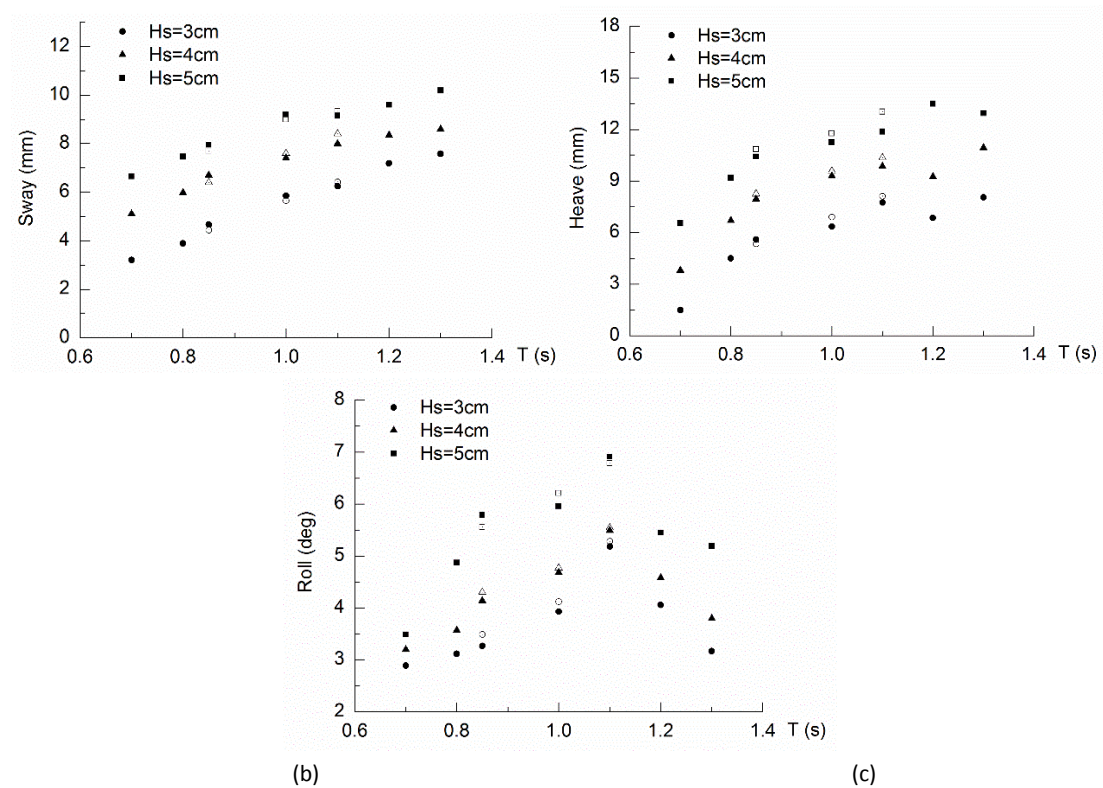


**Fig. 12.** Motion amplitudes of immersed tunnel element suspended by twin-barge with different significant wave heights

#### 4.3 Effect of immersion depth on the tunnel motions

The effect of the immersion depth on the motion response of the tunnel element was also investigated. Given the significant wave height of  $H_s=5\text{cm}$ , Fig. 13 shows the three motion components of the tunnel element with different immersion depths of  $d=0.2\text{m}$ ,  $0.3\text{m}$  and  $0.4\text{m}$ . The results clearly show a decreasing trend of sway and heave motion amplitudes with increasing immersion depth, because wave kinematic amplitudes and hence wave loads on the tunnel decrease with water depth. The motions will also differ due to the increase in pendulum natural period as the suspension lines are increased in length. In this range of the numerical tests, the minimum motion amplitude of the tunnel in the heave direction was  $4.2\text{mm}$  when the immersion depth was  $d=0.4\text{m}$ . When the immersion depth  $d$  was decreased to  $0.2\text{m}$ , the maximum motion amplitude of the tunnel with a large wave period notably increased to  $13.35\text{mm}$ , nearly reach three times of the amplitude at  $T_p=0.7$  with the immersion depth of  $0.4\text{m}$ . For the roll mode, the motion amplitude of the rotation increases with the wave peak frequency period reaching a local maxima at  $T_p=1.1\text{s}$  and then begins to decrease, for all three different immersion depths. Therefore, during installation and in particular lowering of the tunnel element, the resonance of the tunnel-barge system should be avoided to prevent large motions of the tunnel-barge system which could affect the accuracy of positioning the tunnel element and perhaps more fundamentally, risk the safety of

the operation.

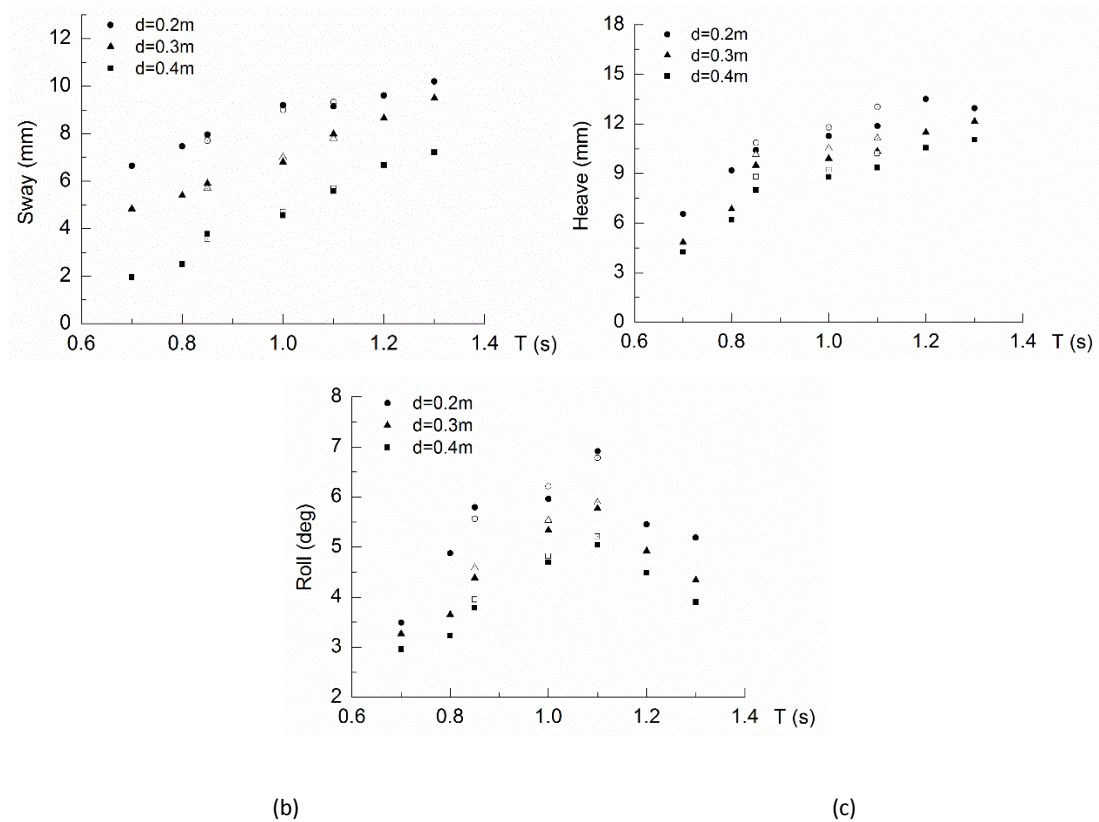


**Fig. 13.** Motion amplitudes of immersed tunnel element suspended by twin-barge with different immersion depths

#### 4.4 Sea states

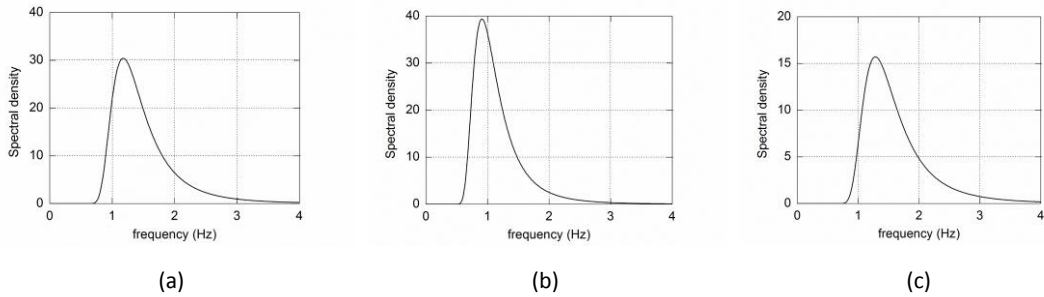
Three typical sea states were chosen to simulate the motion response characteristics of the tunnel element in realistic sea environments (Table 8). The three cases were selected for numerical modelling because: a) the Metocean report gives a 5-year Return Period significant wave height of 1.0m which has been used in the experimental flume tests of Hongkong-Zhuhai-Macao immersed tunnel project by Song et al. (2015); Two different wave periods were considered in Case 1 and Case 2, respectively; and b) Case 3 was chosen with this combination of  $H_s$  and  $T_p$  as it has the highest-frequency of occurrence at the South China Sea sites of interest (Thies et al., 2015).

The full scale environmental values and the wave spectra of these three typical cases are shown in Table 8 and Figure 14, respectively. Comprehensive assessment would require more sea states to be considered however, the three sea states considered in this section are provided as examples of the numerical model capability.

**Table 8**  
Statistical properties of the irregular sea states in numerical model

Case	$H_s$ (m)	$T_p$ (s)	$H_s$ full scale (m)	$T_p$ full scale (s)
1	0.02	0.85	1.0	6

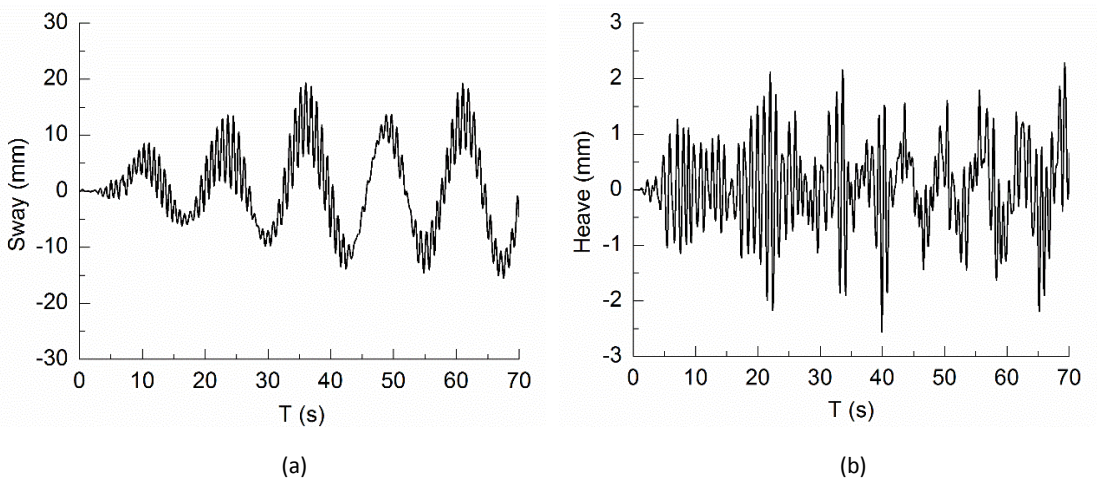
2	0.02	1.1	1.0	7.8
3	0.015	0.78	0.75	5.5



**Fig. 14.** Numerical calculated wave spectrum of three typical cases: a) Case 1, b) Case 2, c) Case 3.

An example of tunnel motion responses simulated by the numerical model and corresponding wave elevation time-series for Case 1 are shown in Fig. 15. The tunnel motion time histories demonstrate strong non-linear characteristics under the influence of irregular wave loading. It can be seen from Fig. 15a that slow-drift forcing influenced the sway motions of the tunnel element suspended by the twin-barge. The mean position of slow-drift oscillation is close to the equilibrium position of the tunnel, with the suspension cables and mooring system contributing to the large low-frequency motion of the tunnel element in wave propagation direction.

Applying the Fast Fourier Transform to the tunnel motion time series with wave peak period of 0.85s in Case 1, Fig. 16a gives the frequency spectral results (black line). The low frequency motion component is demonstrably larger than that caused by first-order wave loading and hence it plays a dominant role in the sway motions of the tunnel element. Taking the sway motion for Case 1 as an example, the frequency of the two extreme value points on the amplitude spectrum curve in Fig. 16a are 0.079Hz and 1.147Hz. The higher frequency corresponds to first-order wave induced motions. The dominant frequency of the other component is 0.079Hz, which is the low frequency motion. The corresponding period is 12.65s and it can also be seen from the time series of sway motions in Fig. 15a.





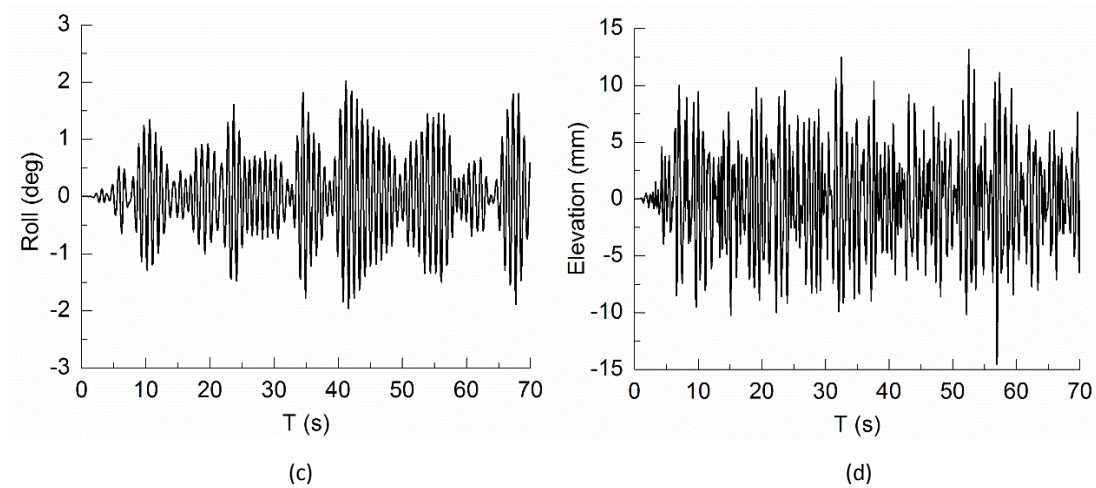


**Fig. 15.** Example of dynamic response time series of tunnel element for Case 1: a) sway motion, b) heave motion, c) roll motion, d) wave elevation

Fig. 16 gives a spectrum analysis comparison of the tunnel motions for three typical cases in realistic sea states. It shows the main tunnel motion harmonics for the sway, heave and roll modes. It can be observed that there are two peaks on the sway motion spectra, and only one dominant peak is observed in the heave and roll motion spectra. The spectra illustrate that the sway motion of the tunnel consists of both low-frequency motion and wave frequency motion, while the dominant motion in heave and roll directions is mainly the wave-frequency motion, as illustrated in Fig. 15a.

For the heave and roll modes, the maximum spectral energy occurs at the wave condition of  $H_s=0.02\text{m}$  and  $T_p=1.1\text{s}$  (Case 2), and conversely the lowest spectra energy is Case 3. This illustrates that for high-frequency motion under the same significant wave height condition, the spectrum density of the tunnel element increases with the wave peak period. Also when the wave periods are relatively close, the larger the significant wave height the greater the spectral energy for the tunnel element. In the sway direction, the same trend is evident for the wave frequency motion of the tunnel. However, for the low-frequency motion, the spectra density value for the tunnel element with Case 1 is larger than that of Case 2, suggesting that the tunnel low-frequency motion plays the dominant role with small wave peak period of Case 1. Fig. 16d also gives the experimental model test results on the motion spectra analysis of the tunnel element based on the wave condition of  $T_p=0.85\text{s}$ ,  $1.0\text{s}$  and  $1.1\text{s}$ . The experimental results show that the spectra peak value of tunnel low-frequency motion decreases with the increasing of wave period, and the spectra density of the tunnel element with the case of  $H_s=0.004\text{m}$  is obviously larger than that of  $H_s=0.003\text{m}$  under the same wave period condition. Overall, the low-frequency drift phenomenon is more apparent at low wave periods for sway tunnel motions, and larger significant wave heights (with more wave energy) will promote drift of the tunnel in the wave propagation direction.

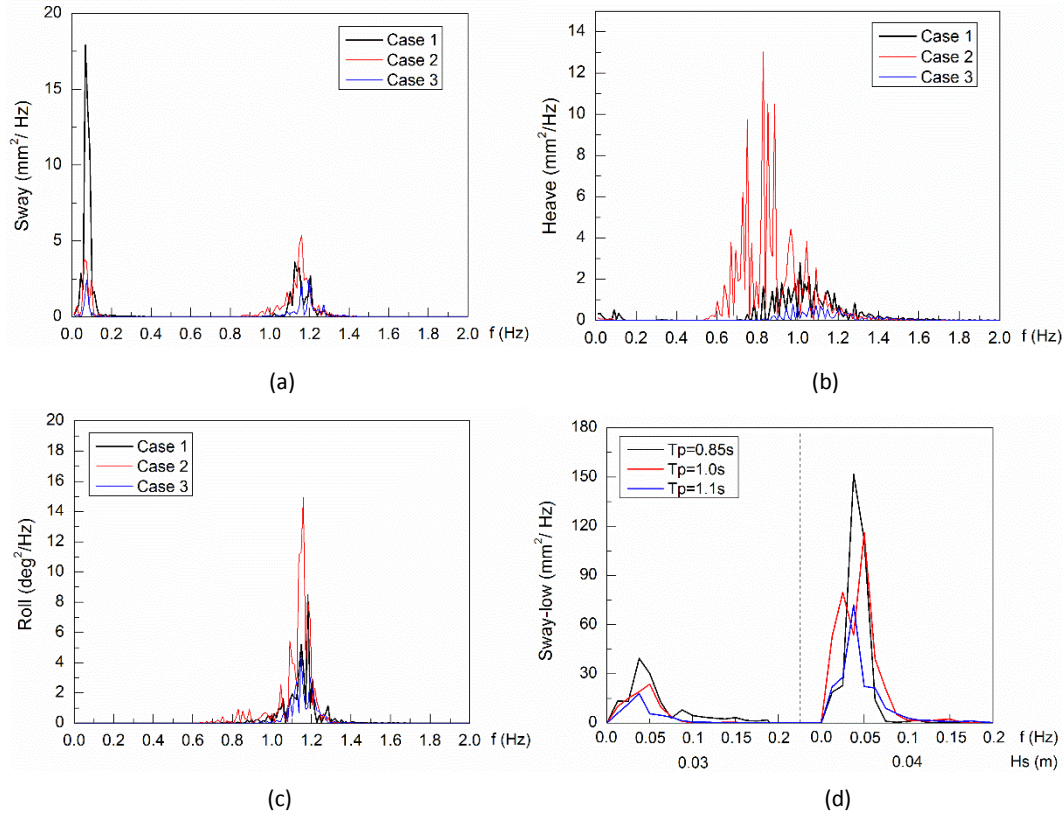


**Fig. 16.** Validation and range extended comparison of motion response of tunnel element for three different wave cases: a) sway motion, b) heave motion, c) roll motion, d) experimental sway motion with the case of  $H_S=0.03\text{m}$  and  $H_S=0.04\text{m}$ .

## 5. Conclusions

In this paper, a comprehensive experimental model has been described to investigate the hydrodynamic characteristics of a tunnel element suspended by a twin-barge subjected to irregular wave conditions. In addition, a detailed validation of the numerical model of tunnel-barge system has been presented. The irregular wave tests carried out and the results compared to numerical simulations of the tunnel-barge system in realistic sea states. Based on the experimental and numerical results, the influence of different wave conditions and the mechanical characteristics of the tunnel-barge system subjected to irregular sea states were discussed.

The results presented in this study clearly demonstrate that the dynamic motions of the twin-barge used to support the tunnel element during transportation and installation should not be ignored. The sway tunnel motions consist of both low- and wave-frequency motions. Comparison of the results for three typical sea states illustrate that the low frequency motion of the tunnel plays the dominant role at small wave peak periods, and tunnel drift increases with increasing significant wave height. Therefore, it is crucial that consideration is made on how to control or limit the low frequency motions of the tunnel and barge during construction procedures and determine which environmental conditions can be classed as safe for transportation and installation procedures.

The sway and heave motion responses of the tunnel element increase with both significant

wave height and wave peak period under irregular wave actions. Tunnel roll motions reached a local maximum at  $T_p=1.1s$  and then started to decrease. This certain period is very close to the natural period of the moored tunnel-barge system. In order to ensure the safety of the installation operation, resonance of the tunnel-barge system should be avoided, particularly at low tunnel immersion depths. Undoubtedly the impact of system natural period on response needs to be considered in practical engineering, and will determine the identification of an appropriate mooring system in order to reduce operational risks.

The numerical model presented in this study will be used for further research: 1) optimization of the mooring system using different materials to investigate their influence on tunnel motions, and study the dynamic behaviour of mooring system in long-term realistic sea states; 2) fully dynamic simulation in regular waves to improve the understanding of resonance mechanism of the tunnel-barge system involved in extreme wave conditions; 3) inclusion of a foundation trench on the seabed to simulate the immersion installation operations; and 4) inclusion of second-order wave effects in the model. The simulation of the lowering procedure itself is possible and will also be experimentally tested.

### **Acknowledgement**

The work is supported by the National Natural Science Foundation of China (Grant No.11272079), the Foundation for Innovative Research Groups of the National Natural Science Foundation of China (Grant No. 51221961) and the China Scholarship Council (award to Yang Can for 1 year's study abroad at the University of Exeter).

### **Reference**

Anastasopoulos I, Gerolymos N, Drosos V, et al. Nonlinear response of deep immersed tunnel to strong seismic shaking [J]. *Journal of Geotechnical and Geoenvironmental Engineering*, 2007, 133(9): 1067-1090.

Aono T, Sumida K, Fujiwara R, et al. Rapid stabilization of the immersed tunnel element[C]. *Proceedings of the Coastal Structures 2003 Conference*. 2003, Portland, Oregon.

Chen, K.Q., Peng, S., Wu, W.G., et al. Model test of immersed tunnel element in towing flume in winds, waves and currents[C]. *Twenty-second Int. Offshore Polar Eng. Conf.*, 2012:831-836.

Chen Z, Wang Y, Wang G, et al. Frequency responses of immersing tunnel element under wave actions [J]. *Journal of Marine Science and Application*, 2009, 8(1): 18-26.

CW Zheng, H Zhuang, X Li and XQ Li, 'Wind energy and wave energy resources assessment in the East China Sea and South China Sea'. *Science China Technological Sciences* 55(1):163-173, 2012

Do N A, Dias D, Oreste P, et al. Behaviour of segmental tunnel linings under seismic loads studied

with the hyperstatic reaction method [J]. *Soil Dynamics and Earthquake Engineering*, 2015, 79: 108-117.

Fu Q.G., 2004. Development and prospect of immersed tunnels. *China Harbor Engineering*, 2004(5), 53-58.

Grantz W C. Immersed tunnel settlements-Part 1: nature of settlements [J]. *Tunnelling and Underground Space Technology*, 2001, 16:195-201.

Guan M.X., 2004. The role of the tunneling by immersed tube method in the river-crossing engineering and some related new cognitions. *Modern Tunneling Technology*, 41(1), 1-2.

Harnois V, Weller S D, Johanning L, et al. Numerical model validation for mooring systems: Method and application for wave energy converters. *Renewable Energy*, 2015, 75: 869-887.

Janssen W, de Haas P, Yoon Y H. Busan-Geoje Link: Immersed tunnel opening new horizons [J]. *Tunnelling and Underground Space Technology*, 2006, 21(3): 332.

Kasper, T., Steenfelt, J. S., Pedersen, L. M., Jackson P. G. & Heijmans, R. W. M. G. (2008). Stability of and Immersed Tunnel in Offshore Conditions under Deep Water Wave Impact. *Coastal Engineering*; 2008, August, 55(9): 753-760.

Li W, Fang Y, Mo H, et al. Model test of immersed tube tunnel foundation treated by sand-flow method [J]. *Tunnelling and Underground Space Technology*, 2014, 40: 102-108.

Li X.B., Wang M.Y. and Qian Q.H., 2003. Development of pipe-sinking tunnels and the pipe-sinking tunnel scheme of Qiongzhou Strait. *Geotechnical Engineering World*, 6(7), 7-11.

Partha C, Zentech, Subrata K. Dynamic simulation of immersion of tunnel elements for Busan-Geoje Fixed Link Project[C]. *Proceedings of the ASME 27 International Conference on Offshore Mechanics and Arctic Engineering*.2008.

Peng, S., Wu, W.G., Chen, K.Q., et al. Experimental investigation on element immersing process of immersed tube tunnel of Hong Kong-Zhu Hai-Macao Bridge[C]. *ASME 31st Int. Conf.*, 2012:1-7.

Sarpkaya T., Isaacson M., 1981. *Mechanics of wave forces on offshore structures*. Van Nostrand Reinhold Company, New York, USA, p.651.

Song Y, Huang G, Zhang N, et al. Experimental study on the mooring tension of tunnel element during immersion standby. *Ocean Engineering*, 2016, 112: 25-32.

Xiao L., Yang J.. Experimental Study on Mooring, Towing and Installing of Immersed Tunnel Caissons [J]. *Shanghai Jiaotong Univ. (Sci.)*, 2010, 5(1):103-107.

Yang C, Wang Y.X., Weller, S., Johanning. L. Experimental Investigation on Hydrodynamic Characteristics of Moored Tunnel Element Suspended by Twin-barge. (Under review)

Yang C, Wang Y., Zuo W.. Numerical simulations on the motion of immersed tunnel element with different arrangement types of mooring lines. The Ocean Engineering, 2014,32 (1),32-40(in Chinese).

Yang C, Wang Y., Zuo W., Ren B. Motion response of immersed tunnel element with mooring lines under irregular wave actions. 36th IAHR World Congress, 28 June – 3 July, 2015, The Hague, the Netherlands.

Zhan D, Wang X. 2001. Experiments of hydrodynamics and stability of immersed tube tunnel on transportation and immersing [J]. J Hydrodynamics B. 2001, 13(2):121–126.

Zhou Y, Jiahua T, Jianmin Y. Experimental investigation on element immersing process of immersed tube tunnel [J]. China Ocean Engineering, 2001 (4): 531-540.